INORGANIC CHEMISTRY
FRONTIERS

RESEARCH ARTICLE

View Article Online
View Journal | View Issue

Cite this: *Inorg. Chem. Front.*, 2022, **9**, 4350

Synergic coordination of multicomponents for the formation of a {Ni_{30}} cluster substituted polyoxometalate and its *in situ* assembly†

Sa-Sa Wang,[a] Xiang-Yu Kong,[a,b] Weiming Wu,[a] Xiao-Yuan Wu,[a] Sheng Cai[a] and Can-Zhong Lu *[a,c]

Developing a new strategy for the synthesis of high-nuclear transition metal (TM) cluster substituted polyoxometalates (POMs) provides an avenue for new materials with unique functions. Herein, the synergetic coordination strategy of 1,2,4-1*H*-triazole (Htrz), ethylenediamine (en), and a lacunary POM was applied to construct a high-nuclear Ni cluster substituted POM. As a result, a {Ni_{30}} cluster substituted POM, **[Ni(trz)$_3$]$_2$@[Ni$_{30}$(H$_2$O)$_{16}$]POM**, representing the highest-nuclear Ni cluster containing POM at present, was discovered for the first time as the secondary building unit (SBU) of four *in situ* assembled frameworks, $[Ni_{11}(trz)_{12}(en)_4(H_2O)_{22}]H_4\{[Ni(trz)_3(H_2O)_3]_2[Ni_{30}(\mu_3\text{-}OH)_{18}(H_2O)_{16}(en)_6(PW_9O_{34})_6]\}\cdot 4Htrz\cdot 222H_2O$ (**1**), $[Ni_6(trz)_6(\mu_3\text{-}OH)(en)(H_2O)_{10}]_2H_8\{[Ni(trz)_3(H_2O)_3]_2[Ni_{30+2}(\mu_3\text{-}OH)_{18}(O)_4(H_2O)_{16}(en)_6(PW_9O_{34})_6]\}\cdot 4Htrz\cdot 94H_2O$ (**2**), $[Ni_{14}(trz)_{12}(en)_6(H_2O)_{36}Cl_2]\{[Ni(trz)_3(H_2O)_3]_2[Ni_{30}(\mu_3\text{-}OH)_{18}(H_2O)_{16}(en)_6(PW_9O_{34})_6]\}\cdot$solvent (**3**), and $[Ni_3(trz)_3(en)(H_2O)_8]_2\{[Ni(en)(H_2O)_2]H_4[Ni_6(\mu_3\text{-}OH)_3(H_2O)_5(en)_3(PW_9O_{34})]\}_2\{[Ni(trz)_3(H_2O)_3]_2[Ni_{30}(\mu_3\text{-}OH)_{18}(H_2O)_{16}(en)_6(PW_9O_{34})_6]\}\cdot 4Htrz\cdot 174H_2O$ (**4**), which served as stable heterogeneous catalysts in light driven hydrogen evolution. The {Ni_{30}} cluster in the SBU held abundant water ligands. On one hand, these water ligands promoted the coordinating assembly of the **[Ni(trz)$_3$]$_2$@[Ni$_{30}$(H$_2$O)$_{16}$]POM** by ligand replacement. On the other hand, they further coordinated with Ni^{2+} to expand the Ni cluster to a larger one. It is believed that the work will trigger tremendous interest in the fields of both synthesis chemistry of POM and hydrogen evolution catalysts.

Received 18th May 2022,
Accepted 3rd July 2022

DOI: 10.1039/d2qi01073a

rsc.li/frontiers-inorganic

Introduction

Developing new materials with unique properties is one of the hottest research topics in the world's science and technology frontier. The structural combination of two clusters leads to not only the combination of their properties, but also adjusting of their properties by each other, and consequently endows the mixed cluster with unique properties. Therefore, the structural combination of two clusters provides an avenue for developing new materials with unique properties. POMs are a class of discrete polyanion clusters with oxo-metal polyhedra of MO_x (x = 5, 6) as the basic construction units. M generally represents early TMs in their high oxidation state including W, Mo, V, Nb, Ta, *etc.*[1] Partial substitution of the polyanion by other oxo-metal clusters results in the production of mixed POM clusters, the properties of which are closely related to the nuclearity and structure of the substituting clusters. Driven by the aesthetically intriguing architectures and promising potential applications of high-nuclear TM cluster substituted POMs in the fields of high-density information storage, single-molecule magnets, nanotechnology, and catalysis, researchers strive for increasing the nuclearity of substituting TM clusters in mixed POM clusters,[2] and substantial efforts have been devoted to the fundamental synthetic work of high-nuclear TM cluster substituted POMs in the past decades. To date, a series of representative TM cluster substituted POMs have been reported, such as $\{Mn_{14}P_4(PW_9)_4\}$,[3] $\{Mn_{19}(SiW_{10})_6\}$,[4] $\{Fe_{12}(P_2W_{15})_4\}$,[5] $\{Fe_{15}P_4(SiW_9)_4\}$,[6] $\{Fe_{16}P_8W_{48}\}$,[7] $\{Co_{16}P_4(PW_9)_4\}$,[8] $\{Co_{16}P_4(XW_9)_4\}$ (X = Si/Ge/P/As),[9] $\{Cu_{15}(SiW_9)_4\}$,[10] $\{Ni_6XW_9\}$ (X = P/Si),[11] $\{Ni_9P_2(PW_9)_3\}$,[12] $\{Ni_{12}W_8(PW_9)_3\}$,[13] $\{Ni_{12}C_3P_4(SiW_9)_3\}$,[14] $\{Ni_{13}P_4(SiW_9)_3\}$,[14] *etc.* However, there are only a few examples with the nuclearity of substituting TM clusters higher than 20 so far, including $\{Fe_{28}(P_2W_{12})_4\}$,[15] $\{Fe_{48}(P_2W_{12})_8\}$,[16] $\{Cu_{20}P_8W_{48}\}$,[17] $\{Ni_{25}C_2P_6(SiW_9)_6\}$,[14] and $\{Zr_{24}W_4(GeW_9)_4(GeW_8)_2\}$.[18] Actually, the

[a]*CAS Key Laboratory of Design and Assembly of Functional Nanostructures, and Fujian Key Laboratory of Nanomaterials, Fujian Institute of Research on the Structure of Matter, Chinese Academy of Sciences, Fuzhou, Fujian 350002, China. E-mail: czlu@fjirsm.ac.cn*
[b]*School of Physical Science and Technology, Shanghai Tech University, Shanghai 201210, China*
[c]*University of Chinese Academy of Science, Beijing 100049, China*

†Electronic supplementary information (ESI) available: Experimental details, Tables S1–S3, Fig. S1–S13, and crystallographic data. CCDC 2093863–2093865 and 2106591. For ESI and crystallographic data in CIF or other electronic format see DOI: https://doi.org/10.1039/d2qi01073a

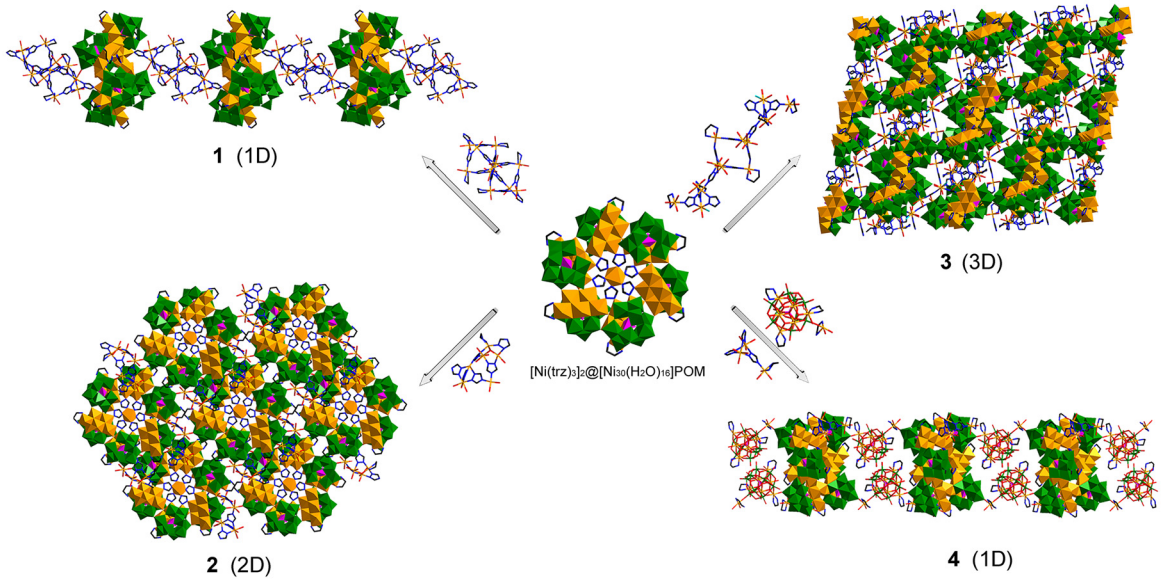

Fig. 1 Crystallographic structure of four frameworks and illustration of their assembly from the SBU **[Ni(trz)$_3$]$_2$@[Ni$_{30}$(H$_2$O)$_{16}$]POM** (color code: orange, Ni; green, W; purple, P; red, O; blue, N; black, C. H atoms have been omitted for clarity).

synthesis of high-nuclear TM cluster substituted POMs is still a formidable challenge.

At present, there are two main synthesis strategies for high-nuclear TM cluster substituted POMs: (1) employing as-prepared large TM clusters stabilized by organic molecules as starting materials; (2) using lacunary POMs as structure directing agents. Sometimes, two strategies are used synchronously.[5,16] Lacunary POMs are regarded as excellent pluridentate inorganic ligands. They can efficaciously gather TM cations into clusters at the lacunary sites. However, the limitations of using pure lacunary POM ligands to construct high-nuclear TM cluster substituted POMs are destined by their confined lacunary space, big size and unusual rigidity. Therefore, the syntheses of most previously reported high-nuclear TM cluster substituted POMs are assisted by small inorganic ligands such as PO_4^{3-},[6,8,9,14,19] CO_3^{2-},[14,20] VO_4^{3-},[19a] AsO_4^{3-},[21] or small organic molecules including AcO^-,[20a,b] ethylenediamine (en)/1,2-diaminopropane (dap),[11] *etc*. However, similar geometries of the above inorganic ligands and sparse coordination sites of the organic ligands make the synthesis of high-nuclear TM cluster substituted POMs progress sluggishly. Keeping this knowledge in mind, we deduce that it is crucial to develop new auxiliary ligands to synergistically coordinate with lacunary POM for the production of high-nuclear TM cluster substituted POMs. Those with dense multiple coordination sites and flexible coordination modes probably act as prospective candidates to break the record of the nuclearity of substituting TM clusters in POMs. Azoles meet these criteria well. Furthermore, azoles take the advantage of similar size to the aforementioned inorganic ligands. For instance, the maximum distance between two non-hydrogen atoms of azole is about 2.2 Å. The value matches well with the size of CO_3^{2-} (the distance between two O atoms is *ca.* 2.2 Å).[22] The synergic coordination of lacunary POMs and azoles is expected to provide more opportunities for the formation of high-nuclear TM cluster substituted POMs. However, relevant studies have not yet been reported.

In this work, the synergic coordination strategy of Htrz, en, and trilacunary phosphotungstate $Na_9[A\text{-}\alpha\text{-}PW_9O_{34}]$ (Na_9PW_9) was employed to construct high-nuclear Ni cluster substituted POMs. As a result, an unprecedented windmill-shaped {Ni$_{30}$} cluster substituted POM, **[Ni(trz)$_3$]$_2$@[Ni$_{30}$(H$_2$O)$_{16}$]POM**, was triumphantly achieved as the secondary building unit (SBU) of four frameworks ranging from one-dimension to three-dimensions, **1–4** (Fig. 1). To the best of our knowledge, the {Ni$_{30}$} cluster represents the highest nuclearity of the Ni cluster in the POM at present. The coordinating assembly of the **[Ni(trz)$_3$]$_2$@[Ni$_{30}$(H$_2$O)$_{16}$]POM** into **1–4** was realized *via* the *in situ* formation and tailoring of organometallic fragments or decorated POMs. The catalytic performances of these compounds in the light driven hydrogen evolution reaction (HER) were carried out, except compound **3** which was restricted by the extremely low yield. The results indicated that they efficaciously promoted the reaction as heterogeneous catalysts under the irradiation of visible light (≥420 nm).

Results and discussion

Formation of the [Ni(trz)$_3$]$_2$@[Ni$_{30}$(H$_2$O)$_{16}$]POM

Frameworks **1–4** were obtained under hydrothermal conditions from a one-pot reaction of $NiCl_2{\cdot}6H_2O$ with Htrz, en, and Na_9PW_9. Their crystallographic data are presented in Table S1.† The TG curves of **1**, **2**, and **4** suggested that their

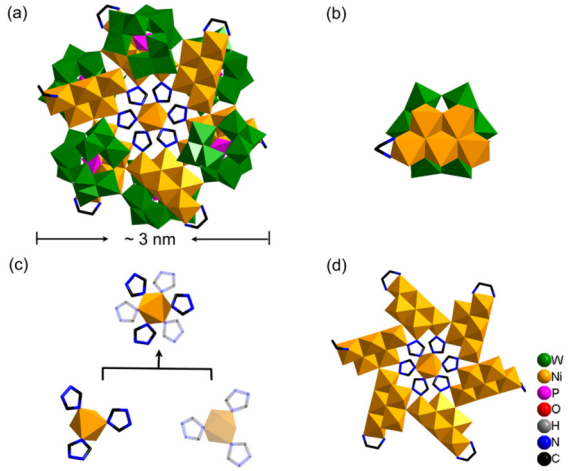

Fig. 2 (a) Structure of the SBU **[Ni(trz)$_3$]$_2$@[Ni$_{30}$(H$_2$O)$_{16}$]POM**; (b) Ni$_5$POM fragment; (c) [Ni(trz)$_3$]$_2$ template in the center of the {Ni$_{30}$} cluster; (d) consecutive rotiform {Ni$_{30}$} cluster in the **[Ni(trz)$_3$]$_2$@[Ni$_{30}$(H$_2$O)$_{16}$]POM**.

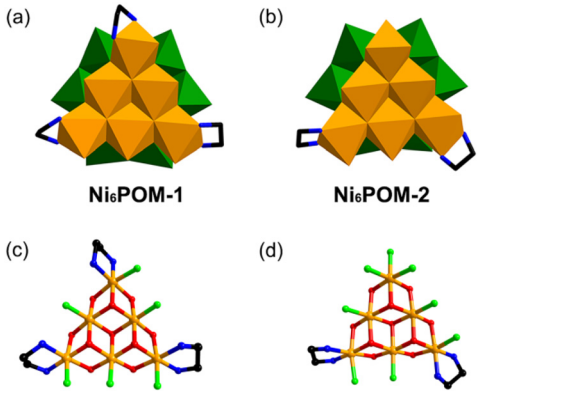

Fig. 3 Structural illustration of (a) **Ni$_6$POM-1**; (b) **Ni$_6$POM-2**; (c) {Ni$_6$} cluster in **Ni$_6$POM-1**; (d) {Ni$_6$} cluster in **Ni$_6$POM-2** (color code: black C; bule N; red O; green O of coordinating water; orange Ni).

decomposition temperatures were around 400 °C, indicating their good thermal stabilities (Fig. S1†). The sharp weight losses before 200 °C were ascribed to the removal of water molecules in the structures. Frameworks **1–4** share a SBU, **[Ni(trz)$_3$]$_2$@[Ni$_{30}$(H$_2$O)$_{16}$]POM**, of ~3 nm diameter, which displays an aesthetic rotiform structure (Fig. 2a). The **[Ni(trz)$_3$]$_2$@[Ni$_{30}$(H$_2$O)$_{16}$]POM** can be viewed as a hexamer of {Ni$_5$}-capped PW$_9$ fragments (**Ni$_5$POM**) alternatingly pointing up and down (Fig. 2b). A floriform moiety consisting of two triangular {Ni(trz)$_3$} complexes arranging in a face-to-face manner with 60° rotation is located in the centre of the **[Ni(trz)$_3$]$_2$@[Ni$_{30}$(H$_2$O)$_{16}$]POM** (Fig. 2c). It is reasonable that the gathering of **Ni$_5$POM** into the **[Ni(trz)$_3$]$_2$@[Ni$_{30}$(H$_2$O)$_{16}$]POM** has been driven by the *in situ* forming [Ni(trz)$_3$]$_2$ moiety. The large {Ni$_{30}$} cluster in the **[Ni(trz)$_3$]$_2$@[Ni$_{30}$(H$_2$O)$_{16}$]POM** assembling from six planar {Ni$_5$} clusters represents the largest Ni cluster in the POM at present (Fig. 2d). It can be speculated that the **Ni$_5$POM** is a metastable species in the present reaction and its stability is significantly inferior to previously reported **Ni$_6$POMs** containing a triangular {Ni$_6$} cluster (Fig. 3).[23] As far as we know, discrete **Ni$_5$POM** species have not been isolated. It is apparent that the shape of the subcluster {Ni$_5$} is identical to that of the {Ni$_6$} cluster in **Ni$_6$POMs** except for the loss of one vertex, which makes it possible to assemble the subunit into a larger Ni cluster.[24] In fact, the production of **1–4** in our system was fiercely competed by **Ni$_6$POM-1** and **Ni$_6$POM-2**, suggesting that the **[Ni(trz)$_3$]$_2$@[Ni$_{30}$(H$_2$O)$_{16}$]POM** and **Ni$_6$POMs** might share the same intermediate **Ni$_5$POM**. Namely, the triangular {Ni$_6$} cluster may also evolve from the metastable {Ni$_5$} cluster. In the absence of *in situ* forming [Ni(trz)$_3$]$_2$, {Ni$_5$} prefers to assemble into {Ni$_6$}, rather than {Ni$_{30}$}. The appearance of [Ni(trz)$_3$]$_2$ breaks the original assembling balance. The speculation was also confirmed by the formation of a hexamer of **Ni$_6$POM** (denoted as **[Ni$_6$POM]$_6$** for convenient description) reported by Kortz, which showed a similar profile to the **[Ni(trz)$_3$]$_2$@[Ni$_{30}$(H$_2$O)$_{16}$]POM** but left the centre of the framework hollow (Fig. S2a†).[25] It is worth emphasizing that the six {Ni$_6$} clusters in **[Ni$_6$POM]$_6$** are discrete despite the use of a dinuclear coordination complex [Ni$_2$(μ-OH$_2$)(O$_2$CCMe$_3$)$_4$(HO$_2$CCMe$_3$)$_4$] as the nickel source. In **[Ni$_6$POM]$_6$**, neighbouring **Ni$_6$POMs** connect with each other *via* four-fold Ni–O=W and two-fold Ni–O–W linkers, attesting to the high activity of the O atoms on the surface of the POM (Fig. S2b†). However, the neighbouring **Ni$_5$POM** fragments in the **[Ni(trz)$_3$]$_2$@[Ni$_{30}$(H$_2$O)$_{16}$]POM** are connected together through Ni–O=W and Ni–O–Ni linkers (Fig. S3†). Additionally, two Ni^{2+} ions respectively belonging to two neighbouring **Ni$_5$POMs** are further bound by a trz of the [Ni(trz)$_3$] complex, improving the interaction between the neighbouring fragments. The fact further suggests the pivotal role of the [Ni(trz)$_3$]$_2$ moiety in the formation of the **[Ni(trz)$_3$]$_2$@[Ni$_{30}$(H$_2$O)$_{16}$]POM**.

The {Ni$_{30}$} cluster in the **[Ni(trz)$_3$]$_2$@[Ni$_{30}$(H$_2$O)$_{16}$]POM** presents a six-segment windmill shape, the cusps of which are coordinated by six en molecules (Fig. 2d). From the overall point of view, the {Ni$_{30}$} cluster is sandwiched by six PW$_9$ fragments from two sides. We hypothesize that the formation of the {Ni$_5$} cluster is cooperatively facilitated by PW$_9$ and en, and the assembly of them into a larger {Ni$_{30}$} cluster should be attributed to the template of the triangular [Ni(trz)$_3$] complexes. In brief, the synergic coordination of trz, en, and PW$_9$ results in the formation of the {Ni$_{30}$} cluster. It is believed that the formation of the triangular [Ni(trz)$_3$] in the centre of the **[Ni(trz)$_3$]$_2$@[Ni$_{30}$(H$_2$O)$_{16}$]POM** is not accidental. Its size well matches that of the pore entrapped by six **Ni$_5$POM** fragments. In order to further confirm the role of en and trz in the formation of the {Ni$_{30}$} cluster, the reactions for **1–4** were carried out in the absence of en or Htrz. As was expected, no {Ni$_{30}$} or {Ni$_5$} cluster containing compounds were found in these reactions. Therefore, both en and Htrz are indispensable for the formation of the {Ni$_{30}$} cluster. Furthermore, a close inspection of the {Ni$_{30}$} cluster in the **[Ni(trz)$_3$]$_2$@[Ni$_{30}$(H$_2$O)$_{16}$]POM** reveals that each of them comprises 18 ternary quasi-cubane {Ni$_3$O$_4$} units counting the shared atoms. Such {Ni$_3$O$_4$} or

$\{Ni_4O_4\}$ subunits are well-known in POM chemistry and closely related to their properties.[19a,26]

In situ coordinating assembly of the $[Ni(trz)_3]_2@[Ni_{30}(H_2O)_{16}]$ POM

The structural combination of POMs and metal–organic frameworks (MOFs) not only integrates their advantages into the resulting framework, but probably endows the framework with extra unique properties such as high stability. The further assembly of the giant **$[Ni(trz)_3]_2@[Ni_{30}(H_2O)_{16}]$POM** into frameworks **1–4** is achieved by *in situ* tailoring of metal–organic bridges or other decorated POMs, rather than expensive large organic ligands, *via* the coordination of $\{Ni_{30}\}$ clusters with trz molecules in bridges and/or the coordination of terminal oxygen atoms on the surface of the **$[Ni(trz)_3]_2@[Ni_{30}(H_2O)_{16}]$POM** with Ni^{2+} ions in bridges. As mentioned before, the formation of the **$[Ni(trz)_3]_2@[Ni_{30}(H_2O)_{16}]$POM** was fiercely competed by discrete **Ni_6POM-1** and **Ni_6POM-2**, which hold 6 and 8 water ligands by the $\{Ni_6\}$ cluster, respectively (Fig. 3c and d).[23] But the yields of **1–4** can be improved by meticulously optimizing the reaction conditions including the dosage of en, the amount of water and the reaction temperature.[27] The structural information of **1–4** reveals that the $\{Ni_{30}\}$ cluster in the **$[Ni(trz)_3]_2@[Ni_{30}(H_2O)_{16}]$POM** holds 16 residual coordinated water molecules (Fig. 4). According to the fact that several frameworks with **Ni_6POM** units as the SBU have been achieved through the replacement of the water ligand by organics,[28] the formation of **1–4** is rationalized by undergoing the same procedure. Therefore, the $\{Ni_{30}\}$ cluster in the **$[Ni(trz)_3]_2@[Ni_{30}(H_2O)_{16}]$POM** may initially hold 18 ternary water ligands before assembling into frameworks **1–4**, which equally distribute on six $\{Ni_5\}$ subclusters and can also be replaced by other ligands (Fig. S4†). But only two of them are replaced by bridges to form **1–4**. It is noteworthy that the distribution and orientation of 16 residual water ligands on the $\{Ni_{30}\}$ cluster are distinguishing for each framework, implying that they may derive from different primitive patterns of the $\{Ni_{30}\}$ cluster (Fig. S4†) and multifold replacement modes possibly occur.

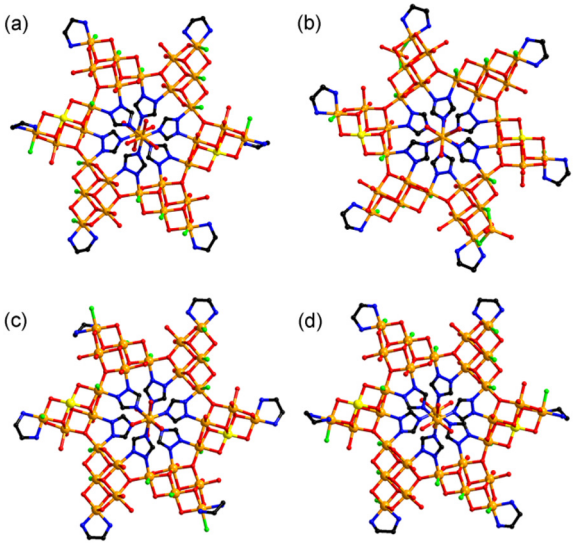

Fig. 4 The substitution mode of water ligands in (a) **1**, (b) **2**, (c) **3**, and (d) **4**. (color code: black, C; blue, N; red, O; green, O of coordinating water; orange, Ni; yellow, Ni coordinating with a bridge).

It is interesting that the **$[Ni(trz)_3]_2@[Ni_{30}(H_2O)_{16}]$POM** was found as the SBU of **1–4**, while **Ni_6POM-1** and **Ni_6POM-2** were detected as discrete structures in our reaction system. The **Ni_6POM**-based framework was absent throughout the work, suggesting that the **$[Ni(trz)_3]_2@[Ni_{30}(H_2O)_{18}]$POM** is more active than **Ni_6POMs**. The assembling behaviour by ligand replacement commenced immediately once the **$[Ni(trz)_3]_2@[Ni_{30}(H_2O)_{18}]$POM** formed. Actually, we have tried to synthesize the discrete **$[Ni(trz)_3]_2@[Ni_{30}(H_2O)_{18}]$POM** by optimizing the reaction temperature and input ratio of the starting materials. But the results were disappointing. Besides, decreasing the coordination capacity of Htrz by introducing a sterically hindered substituent group to prevent the **$[Ni(trz)_3]_2@[Ni_{30}(H_2O)_{18}]$POM** from assembling into frameworks was also carried out. Unfortunately, we failed again when 3-methyl-1*H*-1,2,4-triazole and 3-amino-1*H*-1,2,4-triazole were used instead of Htrz. These results can be rationalized by the high activity of the **$[Ni(trz)_3]_2@[Ni_{30}(H_2O)_{18}]$POM** originating from numerous active terminal O atoms on its surface and multiple commutable water ligands on the $\{Ni_{30}\}$ cluster. It is believed that more frameworks with the **$[Ni(trz)_3]_2@[Ni_{30}(H_2O)_{18}]$POM** as the SBU can be expected in the future.

Framework **1** was initially obtained at 160 °C. It crystallized in the triclinic $P\bar{1}$ space group and was found as a one-dimensional chain structure. In **1**, the **$[Ni(trz)_3]_2@[Ni_{30}(H_2O)_{16}]$POM** is bridged by *in situ* formation of a metal–organic fragment $[Ni_{11}(trz)_{12}]$, which contributes two Ni^{2+} ions (yellow in Fig. S5,† left) and two N atoms (dark purple, Fig. S5,† left) from two trz anions to coordinate with terminal O atoms of the giant SBU and Ni^{2+} ions from the $\{Ni_{30}\}$ cluster, respectively. As mentioned before, 16 commutable water ligands remain on the $\{Ni_{30}\}$ cluster of **1** (Fig. 4a). For four $\{Ni_5\}$ subclusters, the orientations of three water ligands on each of them are identical, while for the other two $\{Ni_5\}$ subclusters on which one Ni^{2+} coordinating with bridge, two residual water ligands on each of them are nearly perpendicular to each other. Therefore, framework **1** was regarded to derive from the primitive **$[Ni(trz)_3]_2@[Ni_{30}(H_2O)_{18}]$POM** with the water distribution of pattern 1 (Fig. S4a†). It was achieved through the replacement of two coordinated water at opposite sides of the $\{Ni_{30}\}$ cluster in the **$[Ni(trz)_3]_2@[Ni_{30}(H_2O)_{16}]$POM** (Fig. S5,† right). The assembly behaviour profited from both unoccupied coordination sites rooting from the dissociation of water ligands on the $\{Ni_{30}\}$ cluster and the highly active terminal O atoms on the surface of the **$[Ni(trz)_3]_2@[Ni_{30}(H_2O)_{16}]$POM**.

The dosages of the starting materials for **1** and **2** are quite resemblant. When the reaction temperature was elevated to 180 °C, framework **2** became the principal product, accompanied by a small amount of **1**. Framework **2** crystallized in the monoclinic $C2/c$ space group. The *in situ* forming $[Ni_6(trz)_6]$ fragments join **$[Ni(trz)_3]_2@[Ni_{30}(H_2O)_{16}]$POMs** into

an undulating two-dimensional layer through the coordination of Ni^{2+} and trz with terminal O atoms and the $\{Ni_{30}\}$ cluster of the **$[Ni(trz)_3]_2$@$[Ni_{30}(H_2O)_{16}]$POM**, respectively (Fig. 1). Each $[Ni_6(trz)_6]$ connects with three **$[Ni(trz)_3]_2$@$[Ni_{30}(H_2O)_{16}]$POMs** and each **$[Ni(trz)_3]_2$@$[Ni_{30}(H_2O)_{16}]$POM** is bound by six $[Ni_6(trz)_6]$ bridges that can be divided into three groups (labelled as A, B and C) according to different coordination modes (Fig. S6†). Bridge A accepts three terminal O atoms on the SBU surface by four Ni^{2+} ions, one of which develops into a μ_3-O, to form Ni–O–W linkers. Bridge B accepts one terminal O atom on the SBU surface by one Ni^{2+} and donates one N atom from trz to coordinate with the $\{Ni_{30}\}$ cluster. Bridge C connects the SBU by the coordination of one Ni^{2+} ion with one terminal O atom of the SBU. In a word, each $[Ni_6(trz)_6]$ contributes five coordinating sites including one N sites and four Ni sites (Fig. S7†). In framework **2**, two Ni^{2+} ions of the $\{Ni_{30}\}$ cluster and ten terminal O atoms on the surface of the **$[Ni(trz)_3]_2$@$[Ni_{30}(H_2O)_{16}]$POM** participate in the coordination with bridges. The formation of a two-dimensional layer also profited from both the commutable water ligands of the $\{Ni_{30}\}$ cluster and the highly active terminal O atoms of the SBU. It is proposed that the orientations of three water ligands on each $\{Ni_5\}$ subcluster are identical in the primitive $\{Ni_{30}\}$ cluster of **2**, corresponding to pattern 2 of the $\{Ni_{30}\}$ cluster in the **$[Ni(trz)_3]_2$@$[Ni_{30}(H_2O)_{16}]$POM** (Fig. S4b†).

Excitingly, two extra Ni^{2+} ions adhere to the $\{Ni_{30}\}$ cluster in **2** *via* coordinating with two water ligands with an identical orientation to form an expanded $\{Ni_{30+2}\}$ cluster (Fig. 4b), suggesting that a larger Ni cluster can be expected in the present system in the light of numerous water ligands of the $\{Ni_{30}\}$ cluster. In brief, the water ligands on the $\{Ni_{30}\}$ cluster can contribute to the synthesis chemistry of POMs *via* two avenues: forming frameworks by ligand replacement and expanding the Ni cluster in the POM to a larger one, the two most principal branches of POM synthesis chemistry.

Framework **3** was discovered accidentally as the by-product of **1** and only a few crystals were obtained despite the elaborate efforts made to improve the yield. Framework **3** crystallized in the monoclinic $P2_1/n$ space group and showed a compact three-dimensional network that was achieved by a longer $[Ni_{14}(trz)_{12}]$ bridge, which contributed to two N coordinating sites (dark purple, Fig. S8†) and six Ni^{2+} coordinating sites (yellow, Fig. S8†). One $[Ni_{14}(trz)_{12}]$ bridge is bound by six **$[Ni(trz)_3]_2$@$[Ni_{30}(H_2O)_{16}]$POMs** and one **$[Ni(trz)_3]_2$@$[Ni_{30}(H_2O)_{16}]$POM** is also bound by six bridges (Fig. S9†). Framework **3** shares the same primitive form of the **$[Ni(trz)_3]_2$@$[Ni_{30}(H_2O)_{16}]$POM** with **1** (Fig. S4a†), but the replacing sites are apparently different. Two residual coordinating water ligands on the $\{Ni_5\}$ cluster, on which ligand replacement occurs, point to the same orientation (Fig. 4c). Different primitive forms of the **$[Ni(trz)_3]_2$@$[Ni_{30}(H_2O)_{16}]$POM** in **1** and **2** and different replacing sites on the $\{Ni_{30}\}$ clusters between **1** and **3** indicate that more replacing mode of the water ligands on the **$[Ni(trz)_3]_2$@$[Ni_{30}(H_2O)_{18}]$POM** can be expected, suggesting that the **$[Ni(trz)_3]_2$@$[Ni_{30}(H_2O)_{18}]$POM** will be a productive SBU. The structural information of frameworks **1–3** makes it clear that the dimensions of the frameworks are positively correlated with the numbers of coordinating sites provided by $[Ni_x(trz)_y]$ bridges (Table S2†). Thus, multiple coordination sites of *in situ* forming $[Ni_x(trz)_y]$ bridges also play a vital role in the successful realization of high-dimensional **$[Ni(trz)_3]_2$@$[Ni_{30}(H_2O)_{16}]$POM**-based frameworks. Compared to pure large organic ligands, the *in situ* tailoring of $[Ni_x(trz)_y]$ bridges take advantage of apparently low-cost and synchronously holding multiple donor and acceptor coordination sites, providing much more opportunities for assembling such large SBUs into high-dimensional frameworks.

Distinguishing from the case in **1–3**, **$[Ni(trz)_3]_2$@$[Ni_{30}(H_2O)_{16}]$POMs** in chain-like **4** are bridged by $\{Ni_6\}$-capped PW_9 fragments (**Ni_6POM-3**) in pair rather than the $[Ni_x(trz)_y]$ complex (Fig. 1). **Ni_6POM-3** is cognate with **Ni_6POM-1** and **Ni_6POM-2**. Six Ni^{2+} ions of the $\{Ni_6\}$ cluster are also arranged in a triangular shape (Fig. S10a†). An accessional Ni^{2+} ion hangs on the surface of **Ni_6POM-3** *via* W=O–Ni bonds (yellow, Fig. S10a†). The Ni^{2+} ion at one vertex of the triangle and the one hanging on the surface of **Ni_6POM-3** are coordinated by terminal O atoms belonging to two **$[Ni(trz)_3]_2$@$[Ni_{30}(H_2O)_{16}]$POM** units, respectively, to form an infinite chain. The coexistence of two substituted POMs in a structure makes framework **4** quite structurally unique. It also conveys a message that the forming conditions of the **$[Ni(trz)_3]_2$@$[Ni_{30}(H_2O)_{16}]$POM** are very similar to that of **Ni_6POM-3**. The result is in line with the isolation of **Ni_6POM-1** and **Ni_6POM-2** during the preparation of frameworks **1–4**. In framework **4**, although the $\{Ni_{30}\}$ cluster does not participate in the formation of the chain, the replacement of water ligands also occurs. Two $[Ni_3(trz)_3]$ fragments decorate the SBU in **4** *via* ligand replacement (Fig. S10b†). The replacing mode of the $\{Ni_{30}\}$ cluster in **4** is the same as that in **1** (Fig. 4d).

Catalytic performance

The present energy crisis and environmental pollution drive researchers to explore the performance of TM cluster substituted POMs in HERs.[6,29] In particular, Ni cluster substituted POMs have exhibited promising catalytic performance in light driven HERs.[19a,21,30] The UV-VIS-NIR spectra of **1**, **2**, and **4** were recorded before the evaluation of their photocatalytic properties (Fig. 5). The results revealed that they showed strong broad absorption at 200–518 nm, while their precursor Na_9PW_9 only absorbed the light in the ultraviolet region (λ < 350 nm), suggesting the occurrence of ligand-to-metal charge transfer between PW_9 and the $\{Ni_{30}\}$ cluster and confirming the successful regulation of POM's band gap. The enlarged absorption region of **1**, **2**, and **4** will be beneficial for their photocatalytic properties.

Frameworks **1**, **2**, and **4** are insoluble in water and most conventional organic solvents, indicating that they may serve as heterogeneous catalysts in light-driven HERs. HERs with **1**, **2**, and **4** were investigated in acetonitrile with $[Ir(ppy)_2(dtbbpy)]PF_6$ ([Ir]) as the photosensitizer, triethanolamine (TEOA) as the proton donor and 1-benzyl-1,4-dihydronicotinamide (BNAH) as the sacrificial electron donor under the

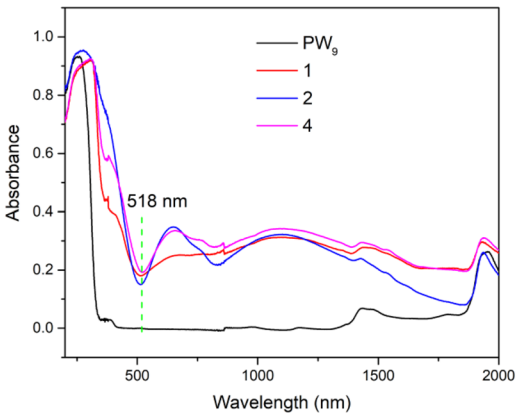

Fig. 5 Comparison of the UV-VIS-NIR spectra of **1**, **2**, and **4** with their precursor Na_9PW_9.

irradiation of visible light ($\lambda \geq 420$ nm). As shown in Fig. 6, when the reaction with **1** was carried out in the dark, no H_2 was detected after 5 h. However, when the reaction was exposed to visible light, H_2 was rapidly generated and the amount reached up to 36.5 μmol in 2 h and the corresponding TON was 56.2, being indicative of the necessity of light. The values for **2** and **4** were 24.4 μmol (TON = 34.1) and 31.1 μmol (TON = 56.9), respectively. These values are comparable to that of previously reported results for H_2 evolution (Table S3†). The better catalytic performances of **1** and **4** than that of **2** can be rationalized by the fully exposed active $\{Ni_{30}\}$ clusters in the 1D chain structures of **1** and **4**. In the absence of a catalyst, the reaction produced a negligible H_2 amount under the irradiation of visible light, further confirming the catalytic function of these frameworks. Equivalent Na_9PW_9, $NiCl_2{\cdot}6H_2O$ and their mixture exhibited extremely low activity under identical conditions. The H_2 amounts for them were less than 3 μmol after 5 h. The results highlighted the benefit of accumulating Ni^{2+} ions at the lacunary sites for photocatalytic properties. The performance of **Ni_6POM-1** in the HER was also investigated. Only 4.9 μmol H_2 was produced in 2 h under identical conditions (TON = 5). The results revealed that it was more inert than **1**, **2**, and **4**.

The time courses of H_2 evolution over **1**, **2**, and **4** showed that the H_2 amount increased rapidly in the initial 1.5 h, and then plateaus were achieved, suggesting that no H_2 was further produced. In order to confirm the retention of catalytic activities of these frameworks, they were recovered by filtration from the reaction mixture after 2 h. After being washed thoroughly with acetonitrile, water and ethanol in succession and then dried naturally, the recovered samples were used in the next reaction. After 5 reaction cycles, no activity loss occurred for these frameworks. Instead, an obvious increasing trend in their activities was presented. The phenomenon was rationalized by the gradual activation of the frameworks. The PXRD patterns of the recovered **1**, **2**, and **4** after 5 reaction cycles were highly consistent with that of the pristine samples (Fig. S11†), being indicative of the maintenance of their struc-

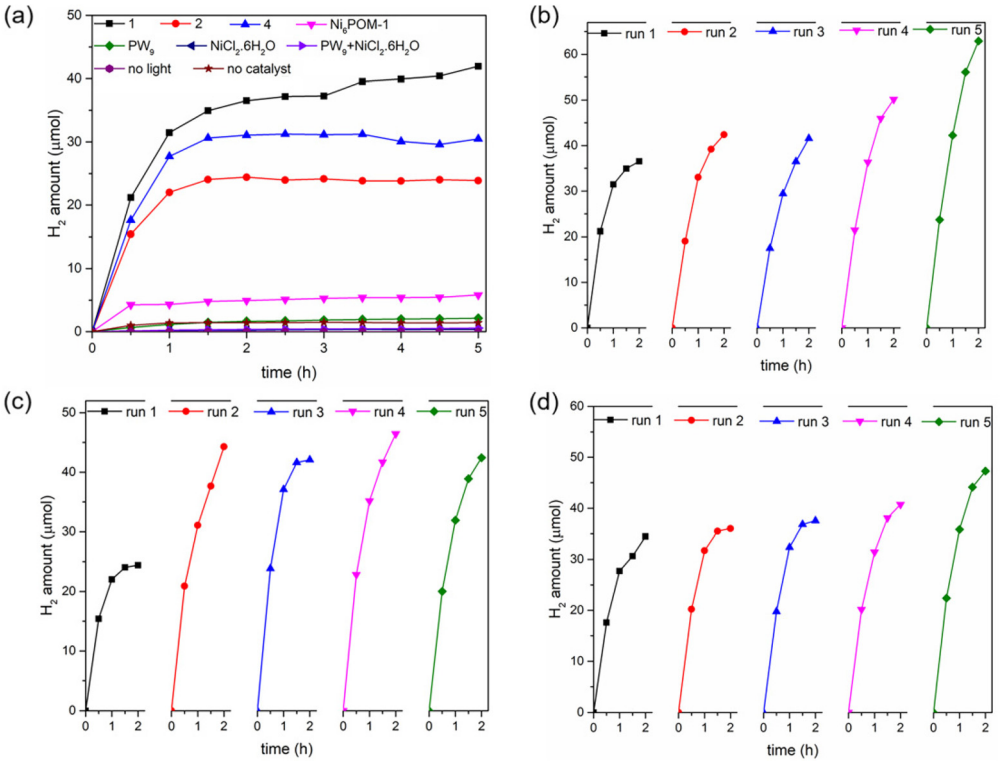

Fig. 6 (a) Time courses of H_2 evolution over different catalysts; recyclability of (b) **1**, (c) **2**, and (d) **4**.

tural integrities, which should be responsible for the retention of catalytic activity.[31] This point was further confirmed by the comparison of the FT-IR spectra of pristine and recovered **1**, **2**, and **4** (Fig. S12†). Therefore, it was deduced that the plateaus with **1**, **2**, and **4** resulted from the deactivation of the photosensitizer, rather than the catalysts. To confirm the supposition, an equivalent photosensitizer [Ir] to that for the initial reaction with **2** was replenished after 2 h. As was expected, the H_2 evolution capacity of the system was totally recovered (Fig. S13†).

Conclusions

In summary, a $\{Ni_{30}\}$ cluster substituted POM, **$[Ni(trz)_3]_2$@$[Ni_{30}(H_2O)_{16}]$POM**, with abundant water ligands on the $\{Ni_{30}\}$ cluster, representing the highest-nuclearity of the Ni cluster in the POM at present, was achieved by synergic coordination of trz, en, and PW_9. The water ligands and highly active surface O atoms of the **$[Ni(trz)_3]_2$@$[Ni_{30}(H_2O)_{16}]$POM** promoted its assembly into frameworks of **1–4**. The water ligands on the $\{Ni_{30}\}$ cluster contribute to the synthesis chemistry of POMs *via* two avenues: forming frameworks by ligand replacement and further coordinating with Ni^{2+} to expand the Ni cluster to a larger one, the two most principal branches of synthesis chemistry of POMs. Frameworks **1**, **2**, and **4** exhibited remarkable activity, excellent stability, and prominent recyclability as heterogeneous catalysts for visible light-driven HERs. It is believed that the work will contribute to the further synthesis of high-nuclear TM cluster substituted POMs, the assembly of giant POMs into extended frameworks, and the development of POM-based hydrogen evolution catalysts.

Conflicts of interest

There are no conflicts to declare.

Acknowledgements

This work was financially supported by the National Natural Science Foundation of China (21773247, 21521061, 21875252) and the Natural Science Foundation of Fujian Province (2006L2005).

Notes and references

1 (*a*) M. Wang, X.-Y. Wu, S.-S. Wang and C.-Z. Lu, A Stable Polyoxometalate-Based Coordination Polymer for Light Driven Degradation of Organic Dye Pollutant, *Chin. J. Struct. Chem.*, 2021, **40**, 1449–1455; (*b*) S.-X. Wang, S.-S. Wang, X.-Y. Wu, W.-B. Yang and C.-Z. Lu, Two Polyoxometalate-Based Host-Guest Compounds: Synthesis, Crystal Structure and Catalytic Performance, *Chin. J. Struct. Chem.*, 2021, **40**, 1655–1660.

2 (*a*) Z. Li, X. X. Li, T. Yang, Z. W. Cai and S. T. Zheng, Four-Shell Polyoxometalates Featuring High-Nuclearity Ln_{26} Clusters: Structural Transformations of Nanoclusters into Frameworks Triggered by Transition-Metal Ions, *Angew. Chem., Int. Ed.*, 2017, **56**, 2664–2669; (*b*) Z.-J. Liu, X.-L. Wang, C. Qin, Z.-M. Zhang, Y.-G. Li, W.-L. Chen and E.-B. Wang, Polyoxometalate-Assisted Synthesis of Transition-Metal Cubane Clusters as Artificial Mimics of the Oxygen-Evolving Center of Photosystem II, *Coord. Chem. Rev.*, 2016, **313**, 94–110.

3 Q. Wu, Y.-G. Li, Y.-H. Wang, E.-B. Wang, Z.-M. Zhang and R. Clérac, Mixed-Valent $\{Mn_{14}\}$ Aggregate Encapsulated by the Inorganic Polyoxometalate Shell: $[Mn^{III13}Mn^{II}O_{12}(PO_4)_4(PW_9O_{34})_4]^{31-}$, *Inorg. Chem.*, 2009, **48**, 1606–1612.

4 B. S. Bassil, M. Ibrahim, R. Al-Oweini, M. Asano, Z. Wang, J. van Tol, N. S. Dalal, K. Y. Choi, R. N. Biboum, B. Keita, L. Nadjo and U. Kortz, A Planar $\{Mn_{19}(OH)_{12}\}^{26+}$ Unit Incorporated in a 60-Tungsto-6-Silicate Polyanion, *Angew. Chem., Int. Ed.*, 2011, **50**, 5961–5964.

5 C. P. Pradeep, D. L. Long, P. Kogerler and L. Cronin, Controlled Assembly and Solution Observation of a 2.6 nm Polyoxometalate 'Super' Tetrahedron Cluster: $[KFe_{12}(OH)_{18}(\alpha\text{-}1,2,3\text{-}P_2W_{15}O_{56})_4]^{29-}$, *Chem. Commun.*, 2007, 4254–4256.

6 T. Cui, L. Qin, F. Fu, X. Xin, H. Li, X. Fang and H. Lv, Pentadecanuclear Fe-Containing Polyoxometalate Catalyst for Visible-Light-Driven Generation of Hydrogen, *Inorg. Chem.*, 2021, **60**, 4124–4132.

7 S. S. Mal, M. H. Dickman, U. Kortz, A. M. Todea, A. Merca, H. Bogge, T. Glaser, A. Muller, S. Nellutla, N. Kaur, J. van Tol, N. S. Dalal, B. Keita and L. Nadjo, Nucleation Process in the Cavity of a 48-Tungstophosphate Wheel Resulting in a 16-Metal-Centre Iron Oxide Nanocluster, *Chem. – Eur. J.*, 2008, **14**, 1186–1195.

8 M. Ibrahim, Y. Lan, B. S. Bassil, Y. Xiang, A. Suchopar, A. K. Powell and U. Kortz, Hexadecacobalt(II)-Containing Polyoxometalate-Based Single-Molecule Magnet, *Angew. Chem., Int. Ed.*, 2011, **50**, 4708–4711.

9 X.-B. Han, Z.-M. Zhang, T. Zhang, Y.-G. Li, W. Lin, W. You, Z.-M. Su and E.-B. Wang, Polyoxometalate-Based Cobalt–Phosphate Molecular Catalysts for Visible Light-Driven Water Oxidation, *J. Am. Chem. Soc.*, 2014, **136**, 5359–5366.

10 B. S. Bassil, A. Haider, M. Ibrahim, A. S. Mougharbel, S. Bhattacharya, J. H. Christian, J. K. Bindra, N. S. Dalal, M. Wang, G. Zhang, B. Keita, I. A. Rutkowska, P. J. Kulesza and U. Kortz, 15-Copper(II)-Containing 36-Tungsto-4-Silicates(IV) $[Cu_{15}O_2(OH)_{10}X(A\text{-}\alpha\text{-}SiW_9O_{34})_4]^{25-}$ (X = Cl, Br): Synthesis, Structure, Magnetic Properties, and Electrocatalytic CO_2 Reduction, *Dalton Trans.*, 2018, **47**, 12439–12448.

11 S. T. Zheng, D. Q. Yuan, H. P. Jia, J. Zhang and G. Y. Yang, Combination between Lacunary Polyoxometalates and High-Nuclear Transition Metal Clusters under Hydrothermal Conditions: I. from Isolated Cluster to 1-D Chain, *Chem. Commun.*, 2007, 1858–1860.

12 J. M. Clemente-Juan, E. Coronado, J. R. Galán-Mascarós and C. J. Gómez-García, Increasing the Nuclearity of

Magnetic Polyoxometalates. Syntheses, Structures, and Magnetic Properties of Salts of the Heteropoly Complexes $[Ni_3(H_2O)_3(P\,W_{10}O_{39})H_2O]^{7-}$, $[Ni_4(H_2O)_2(P\,W_9O_{34})_2]^{10-}$, and $[Ni_9(OH)_3(H_2O)_6(H\,PO_4)_2(PW_9O_{34})_3]^{16-}$, *Inorg. Chem.*, 1999, **38**, 55–63.

13 H. M. Zhang, Y. G. Li, Y. Lu, R. Clerac, Z. M. Zhang, Q. Wu, X. J. Feng and E. B. Wang, A New Ni_{12} Cluster Based on Polyoxometalate Ligands, *Inorg. Chem.*, 2009, **48**, 10889–10891.

14 X. B. Han, Y. G. Li, Z. M. Zhang, H. Q. Tan, Y. Lu and E. B. Wang, Polyoxometalate-Based Nickel Clusters as Visible Light-Driven Water Oxidation Catalysts, *J. Am. Chem. Soc.*, 2015, **137**, 5486–5493.

15 B. Godin, Y. G. Chen, J. Vaissermann, L. Ruhlmann, M. Verdaguer and P. Gouzerh, Coordination Chemistry of the Hexavacant Tungstophosphate $[H_2P_2W_{12}O_{48}]^{12-}$ with Fe (III) Ions: towards Original Structures of Increasing Size and Complexity, *Angew. Chem., Int. Ed.*, 2005, **44**, 3072–3075.

16 J. Goura, B. S. Bassil, J. K. Bindra, I. A. Rutkowska, P. J. Kulesza, N. S. Dalal and U. Kortz, Fe^{III48} -Containing 96-Tungsto-16-Phosphate: Synthesis, Structure, Magnetism and Electrochemistry, *Chem. – Eur. J.*, 2020, **26**, 15821–15824.

17 S. S. Mal and U. Kortz, The Wheel-Shaped Cu_{20} Tungstophosphate $[Cu_{20}Cl(OH)_{24}(H_2O)_{12}(P_8W_{48}O_{184})]^{25-}$ Ion, *Angew. Chem., Int. Ed.*, 2005, **44**, 3777–3780.

18 L. Huang, S. S. Wang, J. W. Zhao, L. Cheng and G. Y. Yang, Synergistic Combination of Multi-Zr^{IV} Cations and Lacunary Keggin Germanotungstates Leading to a Gigantic Zr_{24}-Cluster-Substituted Polyoxometalate, *J. Am. Chem. Soc.*, 2014, **136**, 7637–7642.

19 (*a*) X.-B. Han, C. Qin, X.-L. Wang, Y.-Z. Tan, X.-J. Zhao and E.-B. Wang, Bio-Inspired Assembly of Cubane-Adjustable Polyoxometalate-Based High-Nuclear Nickel Clusters for Visible Light-Driven Hydrogen Evolution, *Appl. Catal., B*, 2017, **211**, 349–356; (*b*) M. Ibrahim, Y. Xiang, B. S. Bassil, Y. Lan, A. K. Powell, P. de Oliveira, B. Keita and U. Kortz, Synthesis, Magnetism, and Electrochemistry of the Ni_{14}- and Ni_5-Containing Heteropolytungstates $[Ni_{14}(OH)_6(H_2O)_{10}(HPO_4)_4(P_2W_{15}O_{56})_4]^{34-}$ and $[Ni_5(OH)_4(H_2O)_4(\beta\text{-}GeW_9O_{34})(\beta\text{-}GeW_8O_{30}(OH))]^{13-}$, *Inorg. Chem.*, 2013, **52**, 8399–8408.

20 (*a*) C. Pichon, P. Mialane, A. Dolbecq, J. Marrot, E. Riviere, B. S. Bassil, U. Kortz, B. Keita, L. Nadjo and F. Secheresse, Octa- and Nonanuclear Nickel(II) Polyoxometalate Clusters: Synthesis and Electrochemical and Magnetic Characterizations, *Inorg. Chem.*, 2008, **47**, 11120–11128; (*b*) L. Lisnard, P. Mialane, A. Dolbecq, J. Marrot, J. M. Clemente-Juan, E. Coronado, B. Keita, P. de Oliveira, L. Nadjo and F. Sécheresse, Effect of Cyanato, Azido, Carboxylato, and Carbonato Ligands on the Formation of Cobalt(II) Polyoxometalates: Characterization, Magnetic, and Electrochemical Studies of Multinuclear Cobalt Clusters, *Chem. – Eur. J.*, 2007, **13**, 3525–3536; (*c*) Z.-M. Zhang, S. Yao, Y.-G. Li, H.-H. Wu, Y.-H. Wang, M. Rouzières, R. Clérac, Z.-M. Su and E.-B. Wang, A Polyoxometalate-Based Single-Molecule Magnet with a Mixed-Valent $\{Mn^{IV2}Mn^{III6}Mn^{II4}\}$ Core, *Chem. Commun.*, 2013, **49**, 2515–2517.

21 H. Lv, Y. Chi, J. van Leusen, P. Kogerler, Z. Chen, J. Bacsa, Y. V. Geletii, W. Guo, T. Lian and C. L. Hill, $[\{Ni_4(OH)_3AsO_4\}_4(B\text{-}\alpha\text{-}PW_9O_{34})_4]^{28-}$: a New Polyoxometalate Structural Family with Catalytic Hydrogen Evolution Activity, *Chem. – Eur. J.*, 2015, **21**, 17363–17370.

22 C. Lian, H. L. Li and G. Y. Yang, A μ-AsO_4-Bridging Hexadecanuclear Ni-Substituted Polyoxotungstate, *Inorg. Chem.*, 2021, **60**, 3996–4003.

23 J. W. Zhao, H. P. Jia, J. Zhang, S. T. Zheng and G. Y. Yang, A Combination of Lacunary Polyoxometalates and High-Nuclear Transition-Metal Clusters under Hydrothermal Conditions. Part II: from Double Cluster, Dimer, and Tetramer to Three-Dimensional Frameworks, *Chem. – Eur. J.*, 2007, **13**, 10030–10045.

24 W. Deng, Q. Zhang and Y. Wang, Polyoxometalates as Efficient Catalysts for Transformations of Cellulose into Platform Chemicals, *Dalton Trans.*, 2012, **41**, 9817–9831.

25 J. Goura, B. S. Bassil, X. Ma, A. Rajan, E. Moreno-Pineda, J. Schnack, M. Ibrahim, A. K. Powell, M. Ruben, J. Wang, L. Ruhlmann and U. Kortz, Ni^{II36} -Containing 54-Tungsto-6-Silicate: Synthesis, Structure, Magnetic and Electrochemical Studies, *Chem. – Eur. J.*, 2021, **27**, 15080–15084.

26 (*a*) A. Das, F. J. Klinke, S. Demeshko, S. Meyer, S. Dechert and F. Meyer, Reversible Solvatomagnetic Effect in Novel Tetranuclear Cubane-Type Ni_4 Complexes and Magnetostructural Correlations For The $[Ni_4(\mu_3\text{-}O)_4]$ Core, *Inorg. Chem.*, 2012, **51**, 8141–8149; (*b*) S. Petit, P. Neugebauer, G. Pilet, G. Chastanet, A. L. Barra, A. B. Antunes, W. Wernsdorfer and D. Luneau, Condensation of a Nickel Tetranuclear Cubane into a Heptanuclear Single-Molecule Magnet, *Inorg. Chem.*, 2012, **51**, 6645–6654.

27 (*a*) B. Ashok, N. Hariram, S. Siengchin and A. V. Rajulu, Modification of Tamarind Fruit Shell Powder with in situ Generated Copper Nanoparticles by Single Step Hydrothermal Method, *J. Bioresour. Bioprod.*, 2020, **5**, 180–185; (*b*) Q. Gao, Z. Liu and J. Li, Research Progress of Soy Protein Adhesive for Wood-Based Composites, *J. For. Eng.*, 2020, **5**, 1–11; (*c*) B. Joseph, V. K. Sagarika, C. Sabu, N. Kalarikkal and S. Thomas, Cellulose Nanocomposites: Fabrication and Biomedical Applications, *J. Bioresour. Bioprod.*, 2020, **5**, 223–237.

28 (*a*) S. T. Zheng, J. Zhang and G. Y. Yang, Designed Synthesis of POM-Organic Frameworks from $\{Ni_6PW_9\}$ Building Blocks under Hydrothermal Conditions, *Angew. Chem., Int. Ed.*, 2008, **47**, 3909–3913; (*b*) S. T. Zheng, J. Zhang, X. X. Li, W. H. Fang and G. Y. Yang, Cubic Polyoxometalate-Organic Molecular Cage, *J. Am. Chem. Soc.*, 2010, **132**, 15102–15103.

29 (*a*) Y. Feng, L. Qin, J. Zhang, F. Fu, H. Li, H. Xiang and H. Lv, Wheel–Shaped Icosanuclear Cu–Containing Polyoxometalate Catalyst: Mechanistic and Stability Studies on Light–Driven Hydrogen Generation, *Chin. J. Catal.*,

2022, **43**, 442–450; (*b*) M. Zhang, H. Li, J. Zhang, H. Lv and G.-Y. Yang, Research Advances of Light-Driven Hydrogen Evolution Using Polyoxometalate-Based Catalysts, *Chin. J. Catal.*, 2021, **42**, 855–871; (*c*) H. Lv, Y. Gao, W. Guo, S. M. Lauinger, Y. Chi, J. Bacsa, K. P. Sullivan, M. Wieliczko, D. G. Musaev and C. L. Hill, Cu-Based Polyoxometalate Catalyst for Efficient Catalytic Hydrogen Evolution, *Inorg. Chem.*, 2016, **55**, 6750–6758; (*d*) H. Lv, J. Song, H. Zhu, Y. V. Geletii, J. Bacsa, C. Zhao, T. Lian, D. G. Musaev and C. L. Hill, Visible-Light-Driven Hydrogen Evolution from Water Using a Noble-Metal-Free Polyoxometalate Catalyst, *J. Catal.*, 2013, **307**, 48–54; (*e*) Z.-M. Su, M. Zhang, Q. An, D. Qin, H.-L. Li, H. Lv, Z. Jia, Q. Zhang and G.-Y. Yang, Synthesis of Two New Copper-Sandwiched Polyoxotungstates and the Influence of Nuclear Number on Catalytic Hydrogen Evolution Activity, *New J. Chem.*, 2020, **44**, 11035–11041; (*f*) W. Wu, T. Teng, X.-Y. Wu, X. Dui, L. Zhang, J. Xiong, L. Wu and C.-Z. Lu, A Cobalt-Based Polyoxometalate Catalyst for Efficient Visible-Light-Driven H_2 Evolution from Water Splitting, *Catal. Commun.*, 2015, **64**, 44–47.

30 (*a*) H. Lv, W. Guo, K. Wu, Z. Chen, J. Bacsa, D. G. Musaev, Y. V. Geletii, S. M. Lauinger, T. Lian and C. L. Hill, A Noble-Metal-Free, Tetra-Nickel Polyoxotungstate Catalyst for Efficient Photocatalytic Hydrogen Evolution, *J. Am. Chem. Soc.*, 2014, **136**, 14015–14018; (*b*) G. Paille, A. Boulmier, A. Bensaid, M. H. Ha-Thi, T. T. Tran, T. Pino, J. Marrot, E. Riviere, C. H. Hendon, O. Oms, M. Gomez-Mingot, M. Fontecave, C. Mellot-Draznieks, A. Dolbecq and P. Mialane, An Unprecedented $\{Ni_{14}SiW_9\}$ Hybrid Polyoxometalate with High Photocatalytic Hydrogen Evolution Activity, *Chem. Commun.*, 2019, **55**, 4166–4169; (*c*) L. Yu, Y. Ding, M. Zheng, H. Chen and J. Zhao, $[\{\beta\text{-}SiNi_2W_{10}O_{36}(OH)_2(H_2O)\}_2]^{12-}$: a Robust Visible Light-Driven Water Oxidation Catalyst Based on Nickel-Containing Polyoxometalate, *Chem. Commun.*, 2016, **52**, 14494–14497; (*d*) W. Guo, H. Lv, J. Bacsa, Y. Gao, J. S. Lee and C. L. Hill, Syntheses, Structural Characterization, and Catalytic Properties of Di- and Trinickel Polyoxometalates, *Inorg. Chem.*, 2016, **55**, 461–466; (*e*) L. Jiao, Y. Dong, X. Xin, L. Qin and H. Lv, Facile Integration of Ni-Substituted Polyoxometalate Catalysts into Mesoporous Light-Responsive Metal-Organic Framework for Effective Photogeneration of Hydrogen, *Appl. Catal., B*, 2021, **291**, 120091.

31 (*a*) K. Yorseng, S. Siengchin, B. Ashok and A. V. Rajulu, Nanocomposite Egg Shell Powder with in situ Generated Silver Nanoparticles Using Inherent Collagen as Reducing Agent, *J. Bioresour. Bioprod.*, 2020, **5**, 101–107; (*b*) G. Feng, Y. Ma, P. Jia, Y. Hu, L. Hu and Y. Zhou, Chemical Synthesis and Application of Vegetable Oil-Based Plasticizers, *J. For. Eng.*, 2020, **5**, 18–28; (*c*) Z. Chen, H. Gao, W. Li, S. Li, S. Liu and J. Li, Research Progress of Biomass-Based OpticaI MateriaIs, *J. For. Eng.*, 2020, **5**, 1–12.

